

Release of WIMS10: A Versatile Reactor Physics Code for Thermal and Fast Systems

B.A. Lindley, T. D. Newton, J. G. Hosking, P. N. Smith, D. J. Powney, B. Tollit, P. J. Smith,
Amec Foster Wheeler
Dorchester, UK
Tel: +44 1305 85120, Email: ben.lindley@amec-fw.com

Abstract –*The WIMS code provides a versatile software package for neutronic calculations, which can be applied to all thermal reactor types including mixed moderator systems. It can provide lattice cell and supercell calculations using a range of flux solution methods to produce the neutronic libraries for use in PANTHER or other whole core analysis codes. With the release of WIMS10, the range of problems which WIMS can solve has been greatly extended. A WIMS/PANTHER calculation route has been developed and validated for part MOX-fuelled PWRs, with calculations showing excellent agreement with 2D core deterministic and Monte Carlo transport solutions. A flexible geometry 3D method of characteristics transport solver, CACTUS3D has been added to the code. CACTUS3D has been benchmarked for a 3D BWR assembly model, and was in good agreement with a direct 172-group solution in the Monte Carlo code MONK. Fast reactor calculations using the ECCO deterministic calculation route have been validated using experimental data from the ZEBRA reactor. Power deposition can be treated through following neutrons and/or photons to their point of interaction. The improved methodology is shown to give more accurate calculation of heat deposition and improve agreement between calculated and measured detector responses for part MOX-fuelled cores.*

I. INTRODUCTION

The WIMS code provides a versatile software package for neutronic calculations, which can be applied to all thermal reactor types including mixed moderator systems. It can provide lattice cell and supercell calculations using a range of flux solution methods to produce the neutronic libraries for use in PANTHER or other whole core analysis codes. With the release of WIMS10, the range of problems which WIMS can solve has been greatly extended. This paper describes the new capabilities available in WIMS10, and presents several examples of its use.

WIMS has been developed over a period of over 50 years, and has typically been used for thermal reactor applications including Advanced Gas-cooled Reactors (AGRs), Pressurized Water Reactors (PWRs), VVERs and RBMKs using a range of solution methods including the method of characteristics and the collision probability method, and the Monte Carlo method through the inbuilt Monte Carlo code MONK.

All developments to WIMS are tested using an automated test tool, which checks modifications to the code against suite of test cases which cover the modules and options within WIMS. Validation has been performed against a range of experimental data (e.g. ORNL critical

spheres [1] and the DIMPLE core [2]) and against other codes, in particular MONK. This is described in a validation manual, which also identifies and explains the differences in calculated results obtained using different versions of WIMS.

New to WIMS10, ECCO [3] has been incorporated into WIMS to allow the treatment of fast spectrum systems. A flexible geometry 3-D method of characteristics transport solver, CACTUS3D has also been added to the code. WIMS10 also includes methods to model particulate fuel in plate, annular and spherical geometry, allowing the treatment of a range of high temperature reactors including pebble bed modular reactors (PBMRs) [4] and prismatic high temperature reactors with gas or liquid salt coolant.

WIMS10 utilizes a 172-group data library for thermal spectrum calculations and a 1968-group data library for fast spectrum calculations. Data libraries including JEF-2.2, JEFF-3.1.2, CENDL-3.1 and ENDF/B7.0 nuclear data evaluations are available in both group structures, with the JEFF-3.2 and ENDFB/7.1 data libraries to be added in the near future.

Treatment of resonance self shielding has been improved through the treatment of materials of different temperatures in different regions of a fuel pin or array using the subgroup method. This can be combined with

calculation of the temperature distribution through the fuel pin or assembly, to allow the fuel temperature distribution and corresponding temperature-dependent cross sections to be determined. This makes possible more accurate calculations, allowing reactor operators to reduce calculation uncertainties, giving opportunities to improve margins, performance and safety.

The WIMS methodology can support recent improvements to PANTHER. PANTHER now contains micro-depletion functionality which allows an improved treatment of history effects by tracking key isotopes and performing corrections to macroscopic cross sections based upon their composition. PANTHER also now contains an embedded supercell methodology for treatment of cores with heterogeneous geometries and material compositions. This is discussed in Section V.

II. 3D METHOD OF CHARACTERISTICS

The extension of the existing 2D method of characteristics solver in WIMS, CACTUS, to full 3D geometries requires explicit tracing of lines along 3D paths. Once the line lengths, and the interception points of lines with internal model boundaries, have been calculated, much of the existing framework of the CACTUS flux solver can be used.

The 3D version of CACTUS uses the fractal geometry package that is also utilized in the Monte Carlo code MONK [5]. This makes it possible to use an identical geometry input in both CACTUS3D and MONK, making it easy to compare the solutions methods and investigate the effect of approximations.

Here, CACTUS is used to model a BWR fuel assembly, with comparison of results with MONK. The ENDF/B7.0 data library is used. The following solution schemes are considered:

- MONK: using continuous energy data libraries.
- MONK: using the WIMS 172-group data library.
- WIMS: first subgroup theory calculations were performed for each 2D axial slice of the model to prepare 172-group cross sections. A 2D calculation was then performed for each 2D slice to condense down to 22 groups. This is the usual procedure in WIMS prior to a 22-group 2D method of characteristics solution. Here, a 3D method of characteristics solution is instead performed using the 22-group cross sections from each slice of the model.

The BWR fuel assembly considered was for a shim rod position in an ABWR core with a GE14 fuel assembly design [6]. The fuel pins had uniform enrichment of 1.9%. The assembly contained partial length fuel rods and axial blankets. A uniform coolant density was assumed and this was varied to generate different cases. The model is shown

in Fig. 1. The model was visualized using the Visual Workshop software package.

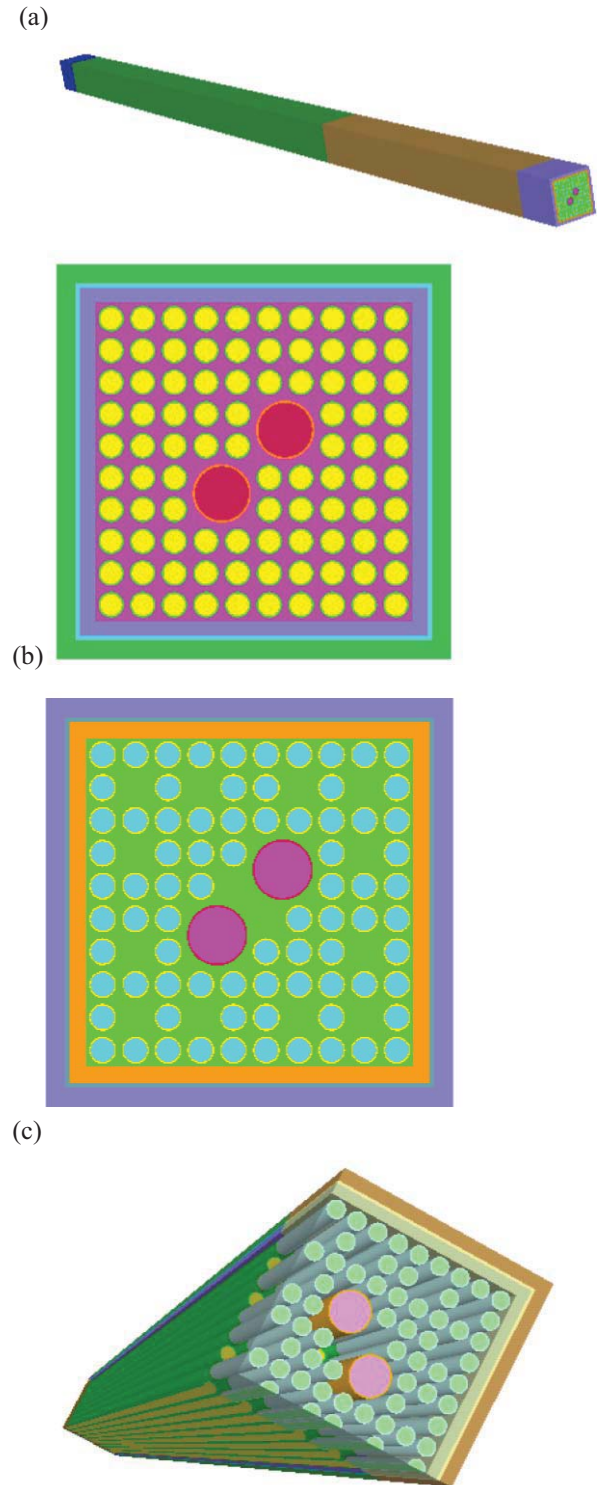


Fig. 1. BWR assembly model. (a) whole model (b) axial plane towards bottom of assembly. (c) axial plane towards top of assembly (d) interface where partial length fuel pins end.

Results for k-infinity are given in Table I. The WIMS methodology was in good agreement with a 172-group calculation in MONK for coolant densities of 0.74 g/cm³ and 0.18 g/cm³. At low water density, the discrepancy between the 172 group data library and the continuous energy data library increased due to limitations of the data library. Work is currently in progress on modifying the WIMS data library to make it more suitable for epithermal spectra applications.

TABLE I
 BWR assembly results

Coolant density (g/cm ³)	0.74	0.46	0.18
k-infinity (MONK continuous energy)	1.2129	1.2171	1.1969
k-infinity (MONK 172 groups)	1.2071	1.2106	1.1890
k-infinity (WIMS)	1.2046	1.2079	1.1896
Discrepancy between MONK 172 groups and WIMS (pcm)	-53	-181	22
Discrepancy between MONK continuous energy and MONK 172 groups (pcm)	-396	-441	-555

The speed and accuracy of the CACTUS3D calculation is controlled by selecting tracking parameters, i.e. the number of azimuthal and polar angles and the spacing between tracks. The geometric regions are also meshed to model the flux variation across the model. The convergence of the model with track spacing is shown in Fig. 2.

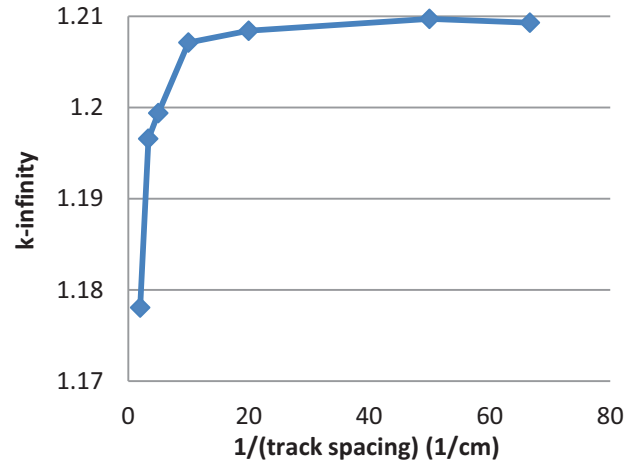


Fig. 2. Convergence of CACTUS3D model with track spacing (40 polar angles, 19 azimuthal angles)

III. FAST REACTOR CALCULATION ROUTE

Fast reactor core calculations can be performed in WIMS10 by utilizing the ECCO cell code in conjunction with the diffusion and 3D method of characteristics solvers. Burn-up calculations can be performed with re-shielding of the key nuclides in ECCO, if desired, while WIMS tracks a wide range of fission product populations. Use of ECCO as part of a calculation route to generate multigroup cross sections for WIMS calculations was validated using k-infinity experiments performed in the ZEBRA zero-power fast reactor at Winfrith, UK [7]. ECCO utilizes a 1968-group data library, and can be used to generate 172-group cross sections, which are suitable for use in further WIMS calculations, for example a whole core solution. Here, to investigate the performance of nuclear data libraries utilized by ECCO and the calculation procedure employed by ECCO, the Monte Carlo code MONK was used to perform a flux solution utilizing the 172-group cross sections generated in ECCO. Calculations were also performed using MONK with continuous energy data BINGO data libraries. The statistical error in MONK was 20 pcm. Calculations were performed with the JEF-2.2, JEFF-3.1.2 and ENDF/B7.0 data libraries to investigate the sensitivity of results to the use of different nuclear data libraries.

The ZEBRA reactor consisted of an array of vertical square stainless steel sheaths in which square plates were stacked horizontally. Each ZEBRA assembly comprised a test region of approximately 60-cm diameter and height, enclosed axially and radially by a 235U-fuelled driver region, further enclosed in a natural-uranium reflector region, 30 cm thick. Both enriched uranium and plutonium fuel plates were used, together with a wide range of non-fissile materials including sodium, steel, aluminium, graphite and natural uranium. The configurations of the 7

ZEBRA experiment configurations considered here are shown in Fig. 3. The plates were ~ 5 cm square and the configurations were ~ 3 – 7 cm in height.

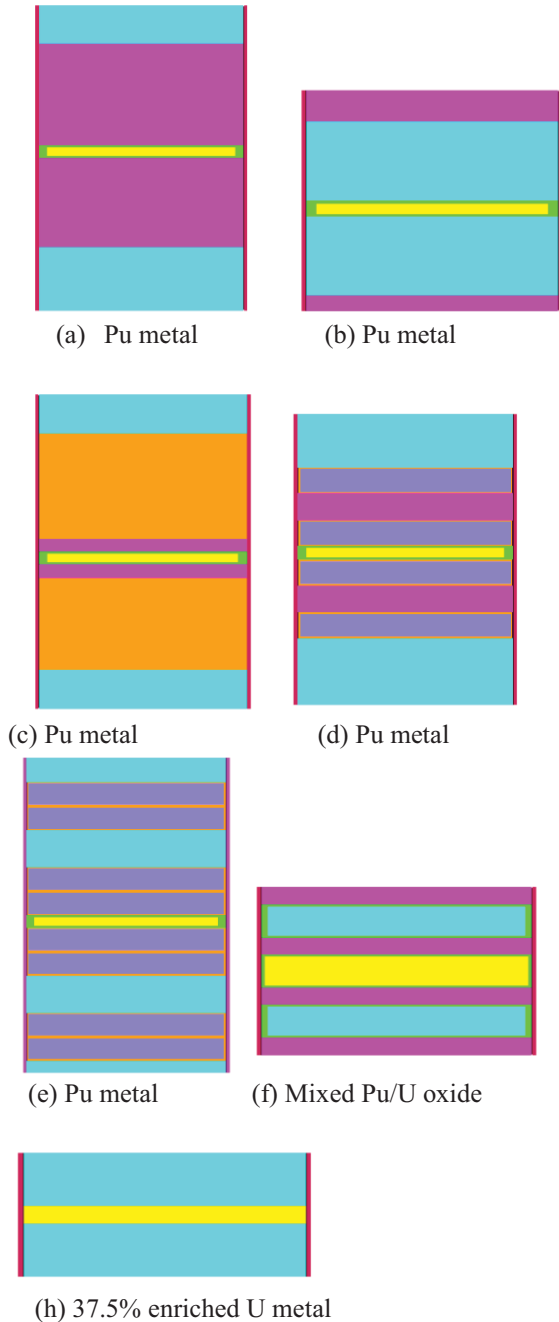


Fig. 3. ZEBRA experiment configurations (yellow = fuel, green = clad, magenta = graphite, cyan = natural uranium, red = sheath, violet = Na, orange = stainless steel/ Na clad). Images produced directly from WIMS/MONK model using Visual Workshop.

There is substantial spectral variation between the 7 configurations, due to varying quantities of metal, oxide and graphite. The spectra for configurations 8A, 8B and 8D are shown in Fig. 4. 8A has a very soft spectrum due to the high proportion of graphite in the system; 8B has a hard spectrum; and 8D has a spectrum similar to that of a fast reactor, with material composition very similar to that of a carbide-fuelled SFR.

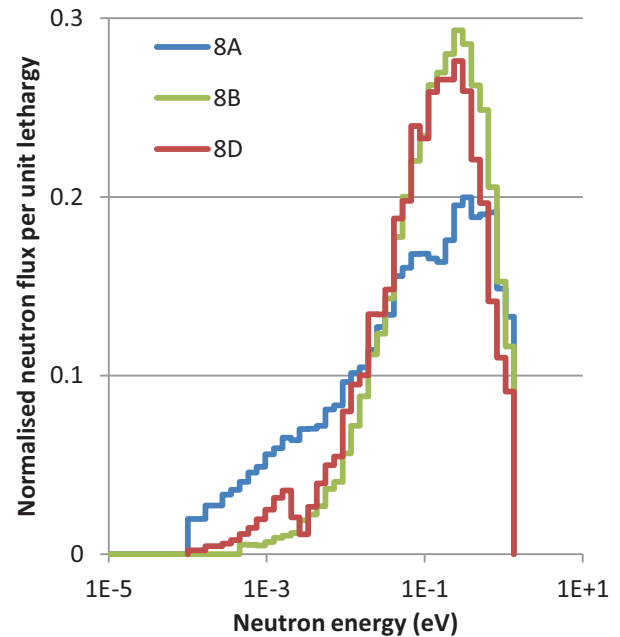


Fig. 4. Experimentally measured spectra for different ZEBRA configurations.

Experimental k-infinity and MONK-calculated k-infinity values with continuous energy data libraries are reported in Table II. Experimental uncertainties and the discrepancies between the MONK results and the experimental values are reported in Table III. MONK generally predicted a lower value of k-infinity than was measured in the experiments.

TABLE II

k-infinity for different data libraries (continuous energy data libraries). Underestimates of k-infinity in MONK are highlighted in blue; overestimates are highlighted in orange.

	Measured	JEF-2.2	JEFF-3.1.2	ENDF/B7.0
8A	0.992	0.9897	0.9885	0.9960
8B	1.001	0.9978	0.9904	0.9917
8C	0.986	0.9786	0.9959	0.9919
8D	0.973	0.9721	0.9723	0.9728
8E	1.006	0.9884	0.9946	0.9880
8F	0.971	0.9641	0.9704	0.9761
8H	1.030	1.0349	1.0166	1.0193

TABLE III

Experimental uncertainty and discrepancies between continuous energy MONK results and experimental values for different data libraries (pcm). Values within the experimental uncertainty are highlighted in green; values outside of the experimental uncertainty range are highlighted in red.

	Measured uncertainty	JEF-2.2	JEFF-3.1.2	ENDF/B7.0
8A	±630	-234	-357	404
8B	±231	-320	-1069	-937
8C	±440	-767	1008	603
8D	±450	-95	-74	-21
8E	±690	-1770	-1139	-1811
8F	±420	-737	-64	538
8H	±251	460	-1280	-1019

The differences between calculations using different nuclear data libraries are substantial, which suggests that the data library is a substantial source of uncertainty for the calculated predictions for these experimental configurations. For Cases 8A and 8D, all data libraries give results that agree with the experiments within 1 standard deviation of experimental uncertainty. For Case 8F, JEFF-3.1.2 agrees well with the experiment, while JEF-2.2 and ENDF/B7.0 substantially overestimate and underestimate k-infinity respectively. For Cases 8C and 8H, some data libraries give results which are too low, while other libraries give results which are too high. For Case 8B, the libraries generally underestimate k-infinity, but JEF-2.2 gives a result within 100 pcm of experimental uncertainty. The largest errors are found for Case 8E, with substantial deviation from experimental values for all 3 data libraries.

To verify that these discrepancies are due to the underlying nuclear data evaluations, calculations were performed for Case 8H in MCNP6 [8] with JEF-2.2 and ENDF/B7, with results in excellent agreement with MONK.

k-infinity values from the ECCO-MONK calculation are shown in Table IV. The discrepancies between ECCO-MONK and continuous energy MONK calculations for different data libraries are given in Table V. The discrepancy between MONK and ECCO-MONK is ~250 pcm on average, which indicates that ECCO can be used to produce multi-group cross sections to a reasonable degree of accuracy for the systems under consideration, for use with the WIMS flux solvers. Some of the configurations had relatively soft spectra, which may reduce the applicability of ECCO and hence contribute towards these discrepancies.

TABLE IV

k-infinity for different data libraries (ECCO-MONK)

	Measured	JEF-2.2	JEFF-3.1.2	ENDF/B7.0
8A	0.992	0.9893	0.9852	0.9916
8B	1.001	0.9990	0.9910	0.9912
8C	0.986	0.9783	0.9943	0.9896
8D	0.973	0.9694	0.9675	0.9679
8E	1.006	0.9842	0.9905	0.9834
8F	0.971	0.9686	0.9726	0.9788
8H	1.030	1.0396	1.0166	1.0197

TABLE V

Discrepancy for ECCO-MONK relative to MONK for different data libraries

	JEF-2.2	JEFF-3.1.2	ENDF/B7.0
8A	-41	-335	-447
8B	120	66	-52
8C	-31	-161	-233
8D	-287	-509	-523
8E	-432	-415	-471
8F	482	232	285
8H	437	2	40

Discrepancies between ECCO-MONK and experimental data are given in Table VI. As for the continuous energy MONK calculations, results for many cases are within experimental uncertainty. In other cases, for the same case both underestimates and overestimates of k-infinity were found for different data libraries. As before, the exception is Case E, for which there is a large deviation from experimental k-infinity. The main difference between this case and other cases is the relatively large proportion of sodium, which provides a significant amount of moderation.

TABLE VI

Experimental uncertainty and discrepancies between ECCO-MONK results and experimental values for different data libraries (pcm). Values within the experimental uncertainty are highlighted in green; values outside of the experimental uncertainty range are highlighted in red.

	Measured uncertainty	JEF-2.2	JEFF-3.1.2	ENDF/B7.0
8A	±630	-275	-692	-42
8B	±231	-200	-1004	-989
8C	±440	-798	848	371
8D	±450	-382	-583	-544
8E	±690	-2202	-1554	-2282
8F	±420	-255	169	824
8H	±251	897	-1278	-979

To investigate the causes of the large data library discrepancies, the ECCO-MONK calculations were rerun

with a mix of cross-sections from different data libraries. Initially, the JEF-2.2 data library was used, and then the ECCO-prepared cross-sections for each isotope in turn were substituted for those from ENDF/B7.0.

TABLE VII

Nuclide contributions of data library discrepancies for ZEBRA: ENDF/B7.0 relative to JEF-2.2. 'Abs' refers to contribution of all neutron absorption reaction. 'Fissile' refers to the fissile material: ^{239}Pu except Case 8H where it is ^{235}U .

	^{238}U Scatter	^{238}U abs	Fissile abs	Remaining difference	Total discrepancy
8A	-322	-84	760	-121	354
8B	-973	-554	683	55	-844
8C	-220	86	814	490*	679
8D	-609	-310	750	7	-169
8E	-765	-266	768	182**	-263
8F	21	-25	762	321**	758
8H	-1129	-640	-113	7	-1882

*includes 260 pcm due to Fe scatter

** includes 179 pcm due to Na scatter

*** includes 183 pcm due to O absorption

Differences in ^{238}U scatter cross section between JEF-2.2 and ENDF/B7.0 can lead to large differences in calculated k-infinity. For the ZEBRA cases, this is particularly true for cases 8B and 8H, where the ^{238}U blanket is in close proximity to the fissile material. Similarly, differences in ^{238}U absorption (combined capture and fission) can lead to JEF-2.2 predicting a significantly higher k-infinity for these two cases than ENDF/B7.0.

For all cases with ^{239}Pu as the fissile material, ~750 pcm of the difference between data libraries is due to differences in the ^{239}Pu capture and fission cross sections between JEF-2.2 and ENDF/B7.0. For the one case with ^{235}U as the driver material (Case 8H), a large difference is not observed.

Therefore, the variation in data library discrepancies between different cases (i.e. whether JEF-2.2 predicts a higher or lower k-infinity than ENDF/B7.0) can largely be explained by the experimental configuration. However, it is not straightforward to identify particular energy ranges in the microscopic cross sections which cause these changes, particularly due to the strong influence of scatter, and this would require further work to determine.

For Case E, calculated k-infinity is somewhat sensitive to choice of Na data library. This was also confirmed for JEFF-3.1 and ENDF/B7.0: use of the JEFF-3.1 Na data library in place of the ENDF/B7.0 Na data library resulted in reactivity 328 pcm higher. Hence one potential reason for the large discrepancy between experimental and measured k-infinity for Case E is the Na scatter cross section.

IV. PHOTON TRANSPORT

Power deposition in WIMS10 can be treated through following neutrons and/or photons to their point of interaction. Photon transport can be treated using a deterministic approach in CACTUS with an isotropic scatter assumption, or using a Monte Carlo approach with explicit treatment of anisotropic scatter.

Pincell test cases were performed to determine the effect of gamma transport on gamma power distribution in the fuel and coolant. Typically, gamma heat makes up around 10% of total heat deposition. While ~98% of neutron heat is deposited in the fuel, only ~80% of gamma heat is deposited in the fuel. Therefore explicit treatment of gamma heating leads to a more accurate calculation of heat deposition in the fuel, with the result that around 96% of heat is deposited in the fuel. The remaining heat is deposited in the clad, coolant and grids. It is important to establish the heat deposition to establish if excessive heating occurs in any components. The distribution of gamma heat deposition is however relatively insensitive to anisotropic scatter effects for these test cases, since they are assumed to be located at the core centre, with a ~0.5% difference in gamma heat deposition in the fuel, which is ~0.05% of total heat deposition.

Explicit treatment of energy deposited in gamma emission and deposition is also necessary to accurately calculate the energy produced through fission. The simplest treatment available in WIMS is to use isotope specific 'Q values' for energy-per-fission and assume all energy (gamma + neutron) is deposited at the point of fission. A more accurate treatment is now available using a coupled neutron and gamma transport calculation. The change in Power per fission with burn-up is shown in Fig. 5 for a simple PWR pincell. This allows more accurate calculation of burn-up dependent assembly powers.

In both cases in Fig. 5 the power per fission increases as the amount of plutonium fission increases. However, the increase for the coupled calculation is greater than that for the Q-value calculation. It is also of note that the power per fission from the Q-value calculation is larger than that from the coupled calculation at the start of life. As Q-values are irradiation independent an average amount of fission products must be assumed in their evaluation. This over estimates fission product contributions at the start of life and under estimates at high irradiation.

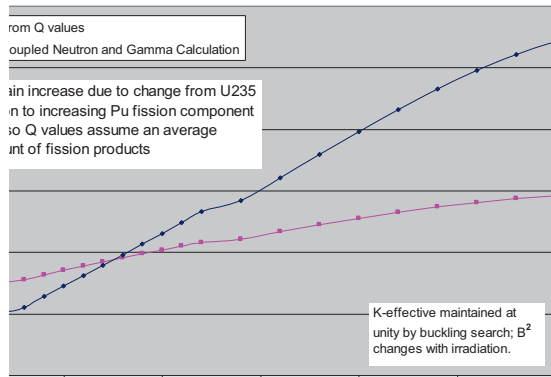


Fig. 5. Power per fission with coupled neutron and gamma calculation.

In addition, at start-of-life, when the fuel is highly reactive, neutrons will leak to other assemblies. At the end of life, neutrons will diffuse from other assemblies into the highly burnt up fuel. Using Q values, where power is deposited at the point of fission, does not allow for this transport of neutron energy. Thus, there will be an over-estimate of power deposition at the start of life and an under-estimate at the end of life. Furthermore, the WIMS Q values are calculated on the basis of compositions containing cycle-average inventories of fission products. Therefore, fission product capture will be over-estimated at start-of-life and under-estimated at end-of-life (leading to an under-estimate of power per fission at start-of-life and vice versa).

The improved heat deposition methodology was applied to treatment of a part MOX-fuelled PWR core. With a neutron transport calculation, the calculated fission rate in the MOX assembly instrumentation tube fission chambers is generally calculated as being about 3% low on average compared to detector measurements. A coupled neutron-gamma transport calculation was therefore performed to determine whether accounting for the gamma response of the fission detector corrects this discrepancy. A supercell model based on the KAIST benchmark [9] was developed and is shown in Fig. 6. The neutron and gamma responses of the detectors in the two assemblies are given in Table VIII.

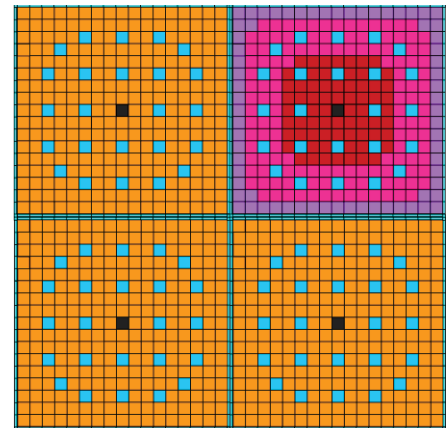


Fig. 6. KAIST supercell model used in coupled neutron-gamma transport calculation.

TABLE VIII

Neutron and gamma responses of detectors in UOX and MOX assemblies (mA)

	UOX	MOX	MOX/UOX
Neutron	0.1936	0.0800	0.413
Gamma	0.0033	0.0032	0.970
Total	0.1969	0.0832	0.423

As postulated, the gamma flux in the UOX and MOX assemblies is almost identical, while the neutron response in the MOX assembly is lower due to the harder neutron spectrum in the MOX assembly. Inclusion of the gamma response increases the relative response of the MOX detector relative to the UOX detector by 2.1%, which is in reasonable agreement with the 3% discrepancy observed.

V. FURTHER DEVELOPMENTS

V.A. Validation for Part MOX-fuelled Cores

A WIMS10 calculation route has been validated for use in part MOX-fuelled PWRs. In WIMS10, 172-group cross sections are first derived using equivalence or subgroup theory. A calculation is performed in 172 groups using a collision probability multicell method. This is used to derive a condensation spectrum for condensing to (typically) 6 groups, for which a detailed transport solution is performed using CACTUS. For UOX and MOX assemblies in part-MOX fuelled cores, a 22-group scheme is instead employed. This route has been validated against reference calculations, with excellent results.

The embedded supercell route in PANTHER allows accurate and rapid treatment of interface effects between assemblies to account for the core heterogeneity in part MOX-fuelled cores [10]. A multigroup pin-by-pin calculation is performed in PANTHER for sets of supercells within the core, with the solution used to derive correction factors for the assembly interface effects for the

core calculation, which is performed using nodal methods. When producing assembly data for a PANTHER calculation, WIMS can be used to simultaneously output multigroup cross-sections for smeared pincells of different types (e.g. fuel, guide tubes, poison pins). Geometric buckling is now treated as an interpolation parameter on the PANTHER nuclear data library, to improve the treatment of embedded supercells that contain reflector regions. This solution method has been benchmarked for 2D core slices by comparison with a deterministic transport solution in CACTUS and a Monte Carlo solution in MONK. Ref. [10] showed that this method could be used to derive pin powers for the KAIST benchmark problem with a maximum pin power error of around 2%.

V.B. Perturbation Calculations and Uncertainty Analysis

Three methods of perturbation analysis are now available in WIMS10 to decompose the change in neutron multiplication factor (k-effective) or reactivity following a perturbation. The first of these is based on collision probabilities, the second uses a diffusion theory perturbation analysis, and the third, by reading in currents generated by CACTUS, can be used for transport theory calculations. Following a collision probability calculation the components of the change in k-effective are output as a function of mesh and as a function of energy group. Following a diffusion theory or transport theory calculation, the components of the change in k are output as a function of reaction (production, absorption, leakage and scatter), as well as by mesh and by energy group.

Further developments are being undertaken to extend the perturbation methods in WIMS to provide a means to obtain the sensitivities associated with k-effective that arise when considering nuclear data. A method has been developed so that perturbations can be applied to cross-sections calculated in WIMS. The method has been developed with the capability to accept a covariance library so that sensitivities can be combined with the covariances to establish the overall uncertainty on k-effective. In burn-up calculations, the input uncertainties affect through-life compositions as well as reactivity or flux. A further sensitivity method is being developed in WIMS that is able to propagate input perturbations so as to obtain the resultant perturbations on compositions at any point during a burn-up calculation. A key advantage of the method is that it enables perturbations affecting burn-up to be quantified efficiently as it applies a direct perturbation to the depletion step, and not to the flux solution.

There are numerous tolerances that apply to the as-manufactured dimensions and compositions of core components. Also, tolerances are used to constrain the variation in components when combined during the assembly of the core. New features are being developed in WIMS to generate perturbed values of input parameters

such as model dimensions and material compositions. Specific components can be sampled so as to meet or fail constraint tests, or to swap or shuffle components so as to meet constraints.

Thus, tools are being developed in WIMS to determine through-life uncertainties on reactor physics parameters that arise from nuclear data as well as perturbations to the reactor core such as changes in geometry and material composition. This makes possible the accurate prediction of calculation and model uncertainties, giving the opportunity to reduce margins, leading to improvements in core performance, operation, and safety.

VI. CONCLUSIONS

The modular structure of WIMS makes it a flexible tool for modeling a range of reactor and core problems. WIMS10 extends the range of problems that WIMS can model, notably through incorporation of the fast reactor cell code ECCO and the 3D method of characteristics solver CACTUS3D.

A WIMS/PANTHER calculation route has been developed and validated for part MOX-fuelled PWRs, with calculations showing excellent agreement with 2D core deterministic and Monte Carlo transport solutions.

CACTUS3D has been benchmarked for a 3D BWR assembly model. An efficient calculation scheme was adopted by preparing 172-group cross sections for 2D axial slices of the model and condensing to 22 groups using a 2D transport calculation, followed by a 22-group 3D method of characteristics solution. For zero to moderate void fractions, the CACTUS3D solutions agreed with the direct 172-group solutions in MONK to within 200 pcm, although the discrepancy was slightly higher for high void fractions.

Cross section preparation for the WIMS10 fast reactor calculation route has been validated using experimental data from the ZEBRA reactor. Accounting for experimental data library uncertainty, there was good agreement between MONK with continuous energy data libraries and the experimental results for 6 of the 7 configurations. ECCO was used to produce multi-group cross sections for the ZEBRA configurations, which allowed reasonably accurate calculation of k-infinity when used in conjunction with a WIMS flux solver. There were significant variations in k-infinity for the ZEBRA configurations between different data libraries for both ECCO and continuous energy MONK calculations.

Power deposition in WIMS10 can be treated through following neutrons and/or photons to their point of interaction using isotropic or anisotropic scatter assumptions. The improved heat deposition methodology was applied to treatment of a part MOX-fuelled PWR core. By performing a gamma transport calculation, it was possible to resolve differences between calculated and

measured detector responses arising when performing a neutron transport calculation only.

Future developments will aim to increase the applicability of WIMS towards whole core calculations including:

- Incorporation of a thermal-hydraulic solver
- Implementation of the SP3 method, and potentially higher order Sn and/or Pn methods, with a transient capability.
- A once-through tracking routine for CACTUS to allow explicit treatment of black boundary conditions in the 3D method-of-characteristics and to allow more uniform spacing of tracks.
- Development of tools to analyze through life uncertainties on reactor physics parameters that arise from nuclear data and perturbations to the reactor core.
- Improve the treatment of epithermal spectrum systems through improved WIMS nuclear data libraries.

References

- [1] R. CHAWLA, "An Assessment of Methods and Data for Predicting Integral Properties for Thermal Reactor Physics Experiments, AEEW-R 797," 1972.
- [2] B. M. FRANKLIN, "The Measurement and Analysis of DIMPLE Benchmark Core, WPC/P151," August 1988.
- [3] G. RIMPAULT, "Algorithmic Features of the ECCO Cell Code for Treating Heterogeneous Fast Reactor Subassemblies," in *International Topical Meeting on Reactor Physics and Computations, Portland, Oregon*, May 1-5, 1995.
- [4] IAEA, "Evaluation of High Temperature Gas Cooled Reactor Performance: Benchmark Analysis Related to the PBMR-400, PBMM, GT-MHR, HTR-10 and the ASTRA Critical Facility," IAEA-TECDOC-1694, 2013.
- [5] S. D. RICHARDS, C. M. J. BAKER, A. J. BIRD, P. COWAN, N. DAVIES, G. P. DOBSON, T. C. FRY, A. KYRIELEIS and P. N. SMITH, "MONK and MCBEND: Current Status and Recent Developments," in *Joint International Conference on Supercomputing in Nuclear Applications and Monte Carlo 2013 (SNA + MC 2013), Paris, France*, October 2013.
- [6] GE NUCLEAR ENERGY, "Advanced Boiling Water Reactor Plant General Description," 2000.
- [7] T. NEWTON, B. FRANKLIN and D. POWNEY, "K-infinity Measurements in ZEBRA Core 8," NEA/NSC/DOC(2011), 2011.
- [8] T. Gorley et al., "Initial MCNP6 Release Overview - MCNP6 Version 1.0," LA-UR 13-22934, 2013.
- [9] KAIST. [Online]. Available: <http://nurapt.kaist.ac.kr/benchmark/>. [Accessed 17 2 15].
- [10] M. KNIGHT, P. BRYCE and S. HALL, "WIMS/PANTHER Analysis of UO2/MOX Cores Using Embedded Supercells," in *PHYSOR 2012*, April 15-20, 2012.
- [11] KAIST, "<http://nurapt.kaist.ac.kr/benchmark/>," [Online]. [Accessed 17 2 15].